$K^*(890)$ and $K^*(1420)$ Production in K^-p Interactions at 4.57 BeV/c†

Y. W. KANG‡
Institute for Atomic Research and Department of Physics, Iowa State University, Ames, Iowa 50010
(Received 10 June 1968)

A study of three-body final states produced in 2-prong K^-p interactions at 4.57 BeV/c is presented on the basis of 10 500 GUTS-fitted events. Abundant production of $K^*(890)$ is observed in all three final states ($K^-\pi^+n$, $\pi^-p\bar{K}^0$, and $K^-p\pi^0$), while $K^*(1420)$ is more copiously produced in the final state $K^-\pi^+n$ than in the others. The spin density matrix elements for the $K^*(890)$ and $K^*(1420)$ are given and the production mechanisms are discussed in terms of the one-meson-exchange model. The cross sections for $K^*(890)$ and $K^*(1420)$ are given.

I. INTRODUCTION

IN this report we present an analysis of K^* production in K^-p interactions at 4.57 BeV/c. The work was carried out at the Brookhaven National Laboratory. The 80-in. hydrogen bubble chamber was exposed in the separated K^- beam at the AGS. The results are based on an analysis of 10 500 measured two-prong events, for which kinematic fits were attempted.

We studied the following reactions:

$$K^-p \to K^-\pi^+n \quad (1)$$

$$\to \pi^-p\bar{K}^0 \quad (2)$$

$$\to K^-p\pi^0, \quad (3)$$

with emphasis on reaction (1). Reaction (1) has been studied by Schweingruber *et al.*[1] at 4.1 and 5.5 BeV/c, Verglas *et al.*[2] at 3.0 BeV/c, and Friedman *et al.*[3] at 1.45 BeV/c.

In the data presented here, the $K^*(890)$ is prominent in all three reactions, while the $K^*(1420)$ is produced more copiously in the final state $K^-\pi^+N$ than in the other final states. The $N^*(1236)$ is observed in reactions (1) and (3).

Isospin considerations indicate that possible exchange particles (in, for example, a one-meson-exchange model) are π and ρ in the $K^{*0}(890)$ production, and π, η, ρ, ω, and ϕ in $K^{*-}(890)$ production. It has been noted by many authors[1,4,5] that η, ρ, and ϕ are relatively less important in $K^*(890)$ production. Thus, both π and ω exchange could occur in the $K^{*-}(890)$ production, but the experimental data[1,4] show dominant ω exchange. This result is consistent with the isospin prediction that for pure $T=1$ pseudoscalar exchange the cross section for $K^{*-}(890)$ is four times as small as that for the $K^{*0}(890)$ production.

We have studied the spin density matrix elements, and the decay angular distributions for the $\bar{K}^{*0}(1420)$, which is strongly produced in reaction (1). A spin-parity assignment of 2^+ is favored.

II. EXPERIMENTAL DETAILS

From a triple scan of approximately 11 000 pictures, a total of 11 500 two-prong events were found in a restricted fiducial volume. Over-all scanning efficiency was 99.5%. All events were measured in three views and reconstructed in space, and 10 500 events were processed with the GUTS kinematic fitting program.[6] Fits to eight likely hypotheses [reactions (1) to (3) plus five other reactions] were attempted with GUTS. A total of 2041 events, which were candidates for one of the three reactions (1) to (3) and were not elastic events, were examined on a scanning table for ionization consistency. Under normal conditions[7] proton-pion and kaon-pion ambiguities could be distinguished up to 1.5 and 0.8 BeV/c, respectively, by comparing with a nearby beam track in at least two views. After a final selection, only 26 of the events included in reaction (1) had a proton-pion ambiguity, and these events were checked individually in the final analysis for particular biases. The χ^2 and missing-mass distribution for the ionization selected events are shown in Fig. 1.

In order to purify the data further, we have used the following criteria for the selection of candidate events:

(1) $P(\chi^2)\geq 1.4\%$, for reaction (1)
$P(\chi^2)\geq 4.6\%$, for reactions (2) and (3)

(2) 1115 MeV > missing mass > 730 MeV for reaction (1),
680 MeV > missing mass > 320 MeV for reaction (2),
400 MeV > missing mass > −300 MeV for reaction (3),

(3) missing-mass error < 500 MeV, and

† Work was performed in part at the Ames Laboratory of the U. S. Atomic Energy Commission. Contribution No. 2331.

‡ Present address: The National Accelerator Laboratory, P.O. Box 500, Batavia, Ill.

[1] F. Schweingruber, M. Derrick, T. Fields, D. Griffiths, L. Hyman, R. J. Jabbur, J. Loken, R. Ammar, R. Davis. W. Kropac, and J. Mott, Phys. Rev. **166**, 1317 (1968).

[2] A. Verglas, S. Focardi, A. Minguzzi-Ranzi, L. Monari, and P. Serra, Nuovo Cimento **41A**, 629 (1966).

[3] A. Friedman, G. Maurer, A. Michalon, B. Schily, R. Strub, G. Zech, and P. Cüer, Phys. Letters **21**, 462 (1966).

[4] S. Goldhaber, J. L. Brown, I. Butterworth, G. Goldhaber, A. A. Hirata, J. A. Kadyk, and G. H. Trilling, Phys. Rev. Letters **15**, 737 (1965).

[5] R. Newman, W. Chinowsky, J. Schultz, W. B. Johnson, and R. R. Larsen, Phys. Rev. **158**, 1310 (1967).

[6] J. P. Berge, F. T. Solmitz, and H. D. Taft, Rev. Sci. Instr. **32**, 538 (1961).

[7] Exceptional cases are steep tracks (>50°), short tracks (<3 cm) due to secondary interactions and poor film conditions. However, these cases were few.

(4) beam tracks must lie within prescribed limits on azimuth, dip, and momentum.

Since at least one of two charged secondaries cannot be identified by ionization alone and fake fits to reactions with more than one neutral particle are possible, a careful investigation of contamination was carried out. We used well-analyzed samples of the four- and five-body final[8] states ($K^-p\pi^+\pi^-$, $K^-p\pi^+\pi^-\pi^0$, and $K^-\pi^+\pi^+\pi^-n$) to create fake two-prong events by treating two of the outgoing charged particles as unmeasured.

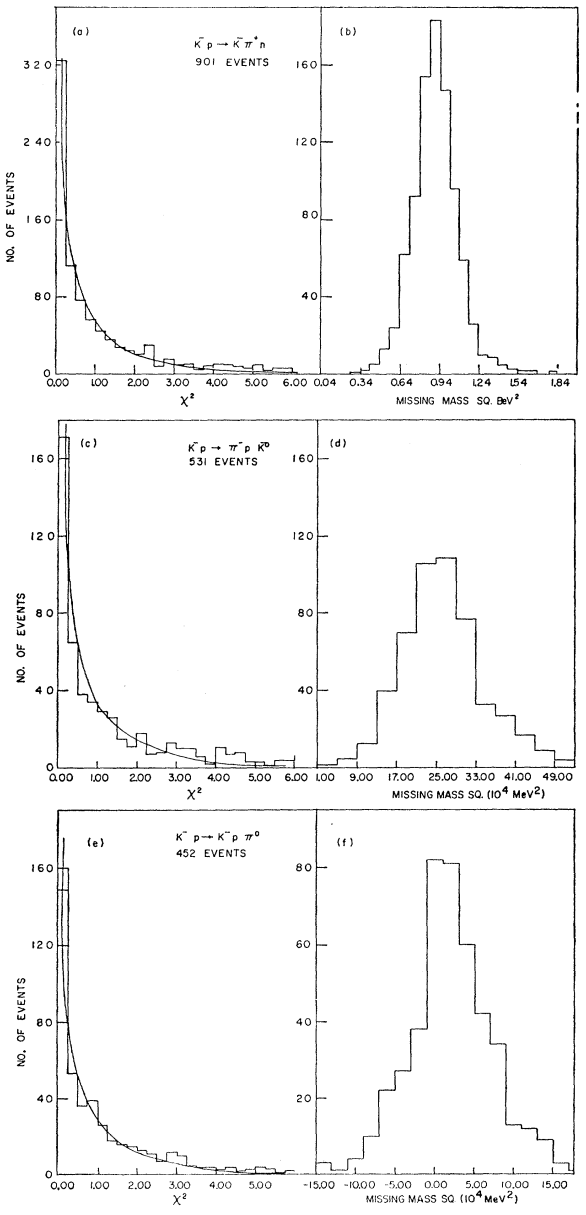

FIG. 1. The X^2 and missing-mass distributions for final states $K^-\pi^+n$, $\pi^-p\bar{K}^0$, and $K^-p\pi^0$.

[8] Roland E. Juhala, Ph.D. thesis, Iowa State University, 1968 (unpublished).

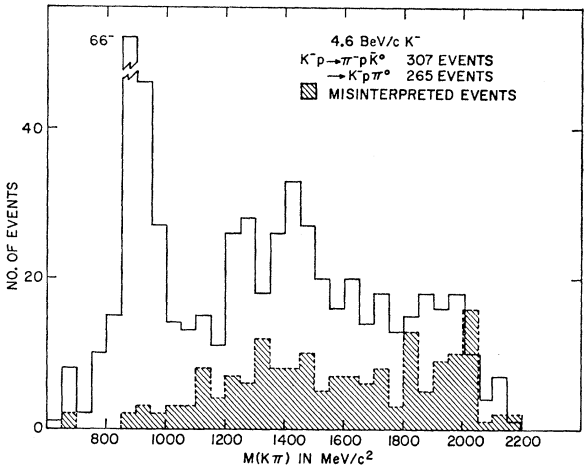

FIG. 2. The $K\pi$ invariant mass distribution for the final states $\pi^-p\bar{K}^0$ and the $K^-p\pi^0$ at 4.6 BeV/c. The shaded area is the background of misidentified events estimated from the $K^-p\pi^+\pi^-$ final state by treating two particles as unmeasured and analyzing them in the same way as actual two-prong events.

These fake two-prong events were then analyzed in the same way as actual two-prong events.[9] We also studied the two-prong–V topology for this purpose. It was found that contamination in reaction (1) is small [$(12\pm4)\%$], while that in reactions (2) and (3) is substantial [$(35\pm10)\%$]. The estimated contamination in reactions (2) and (3) is shown in the $K\pi$ mass projection in Fig. 2. The misidentified events tend to concentrate at higher effective masses. Hence, the $K^{*-}(890)$ is not seriously affected by this background, but the $K^{*-}(1420)$ is likely to be affected substantially. Quantitative investigations in these cases were limited to the $K^{*-}(890)$.

About 14% of the events assigned to reaction (2) were ambiguous with respect to final states (2) and (3) after application of a five-to-one X^2 probability ratio cutoff. This 14% will not significantly affect the final-state analysis, because the $K\pi$ effective mass is essentially invariant under interchange of the meson masses (i.e., K^- to π^- and π^0 to $\bar{K}^0$ or vice versa) when both meson momenta are greater[10] than 1 BeV/c.

Further, when studying the $K^{*-}(890)$ production and decay angular distributions we combined events from reactions (2) and (3) (after separate investigations of the two reactions).

The cross section was determined by computing the K^- path length on the basis of a τ-decay count with corrections for scanning efficiency and for the Dalitz

[9] The dominant contribution to contamination came from four-body final states, and that from five-body final states was negligible. This can be only semiquantitatively interpreted because of uncertainties in cross sections for the final states $K^-p\pi^0\pi^0$, $\pi^-p\bar{K}^0\pi^0$, and $K^-\pi^+n\pi^0$ at 4.57 BeV/c.

[10] About one-half of these ambiguous events could be wrong assignments. These would introduce a bias in angular distributions, but the contribution to the $K^{*-}(890)$ mass region should be small.

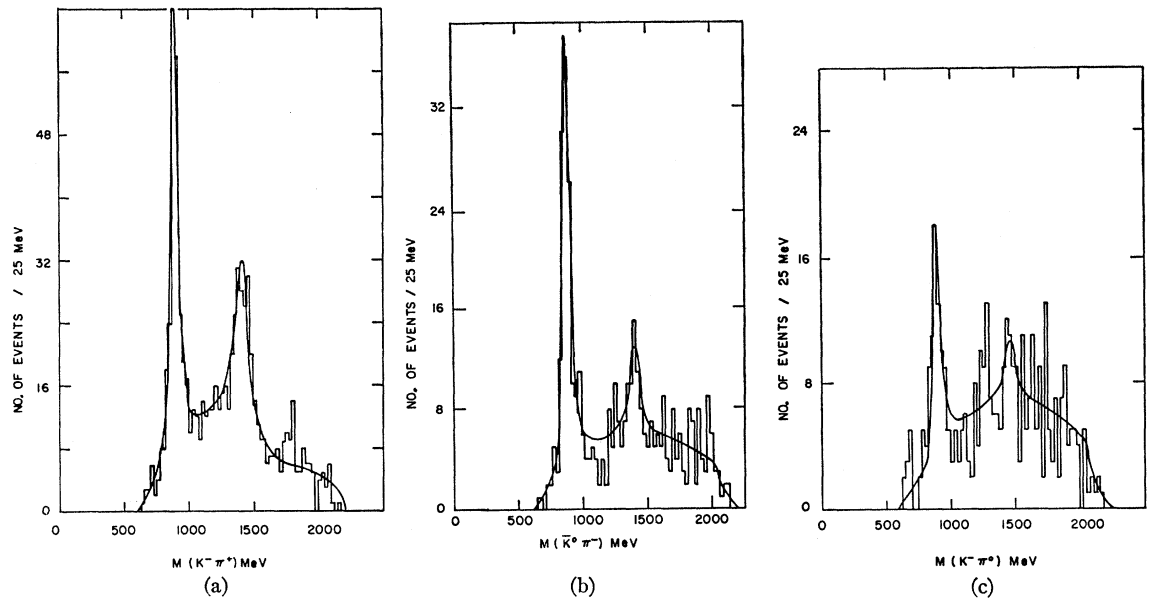

FIG. 3. The $K\pi$ invariant mass distributions: (a) $M(K^-\pi^+)$, (b) $M(\bar{K}^0\pi^-)$, and (c) $M(K^-\pi^0)$.

pair conversion probability of a pion. Using this calculation of the effective K^- path length with the total number of K^-p interactions (determined from a triple scan of part of the film), we obtain a total K^-p cross section in good agreement with counter values.[11] Cross sections in each final state were corrected for unused events which resulted from fiducial volume cuts, measuring failure, and beam track entrance criteria. They were also corrected for background events, pion beam contamination, missing mass, and χ^2 restrictions. Errors in the cross sections include the statistical error and various uncertainties in estimating the cross sections.

III. GENERAL FEATURES OF RESONANCE PRODUCTION

In Figs. 3(a), 3(b), and 3(c) are shown the $K\pi$ invariant mass spectra for reactions (1) through (3), respectively. The $K^*(890)$ is prominent in all three reactions, while the $K^*(1420)$ is produced most copiously in the final state $K^-\pi^+n$. When the $K^*(890)$ mass region is taken from 840 to 940 MeV, the nonresonant backgrounds under the K^* peaks are 18, 12, and 23%, for reactions (1) through (3), respectively. The corresponding background fractions for the

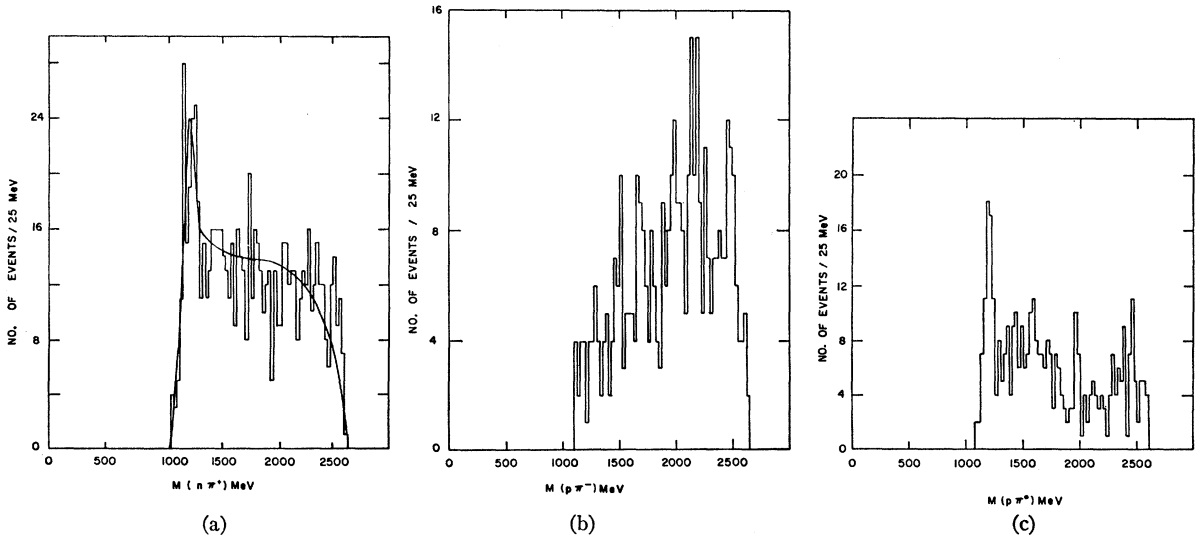

FIG. 4. The $N\pi$ invariant mass distributions: (a) $M(n\pi^+)$, (b) $M(p\pi^-)$, and (c) $M(p\pi^0)$.

[11] W. F. Baker, R. L. Cool, E. W. Jenkins, T. F. Kycia, R. H. Phillips, and A. L. Read, Phys. Rev. **129**, 2285 (1963).

$K^*(1420)$ in the mass region 1330 to 1510 MeV are 41, 64, and 78%, respectively. Figures 4(a), 4(b), and 4(c) show the $N\pi$ invariant mass spectra for reactions (1) to (3), respectively. The $N^*(1236)$ is outstanding in reactions (1) (89 μb) and (3) (36 μb), but is not noticeable in reaction (2), as is the case in other experiments. Over-all resonance production in the three reactions is 52, 40, and 40%, respectively.

In Figs. 5(a), 5(b), and 5(c) are shown Dalitz plots for the $K\pi$ invariant mass versus the $N\pi$ mass in reactions (1) to (3). The $K^*(890)$ band is prominent in all three reactions, while the $K^*(1420)$ is evident in reaction (1) but is less clear in reactions (2) and (3).

In the final states $K^-\pi^+n$ and $K^-p\pi^0$, in which an $N^*(1236)$ enhancement was observed, we observed an asymmetry in the $K^*(890)$ band across the Dalitz plot. We define an asymmetry parameter as the number of events in the lower half of the K^* band minus number of events in the upper half, all divided by the total number of events in the band. The asymmetries for the two final states are $(22\pm7)\%$ and $(28\pm11)\%$, respectively. The asymmetry in reaction (1) is much larger when a four-momentum transfer cut $|t|<0.2$ (BeV/c)^2 is made [see Fig. 9(a)]. The asymmetry appears to be distributed uniformly throughout the lower half of the $K^{*0}(890)$ band. Thus, if one considers this asymmetry to be due to K^*N^* interference, it is necessary to assume interference with more than just the $N^*(1236)$ since the $N^*(1236)$ is confined to the very bottom of the Dalitz plot.

In Figs. 6(a), 6(b), and 6(c) are shown Chew-Low plots. It is evident that $K^*(890)$ and $K^*(1420)$ are produced peripherally, consistent with production by single-meson exchange.

In order to determine the masses, widths, and cross sections of the $K^*(890)$ and $K^{*0}(1420)$, each invariant mass spectrum was fitted with phase space[12] plus two constant-width Breit-Wigner functions (six unknown parameters). The results of these fits are summarized in Table I. The masses and widths agree with accepted values.[13]

The cross sections are also shown in Fig. 7 and compared with other data.[14] Morrison[15] suggested that for quasi-two-body reactions the total cross section decreases as $P_{\text{in}}{}^{-n}$, where P_{in} is the incident beam momentum in the laboratory system and $n\simeq1.5$ for meson exchange. For the $K^*(890)$'s our cross sections are close to the straight line suggested by other data, but the $K^{*0}(1420)$ cross section appears to be a little larger than the value expected from other experiments in the 4- to 6-BeV/c momentum range. It may be that the cross

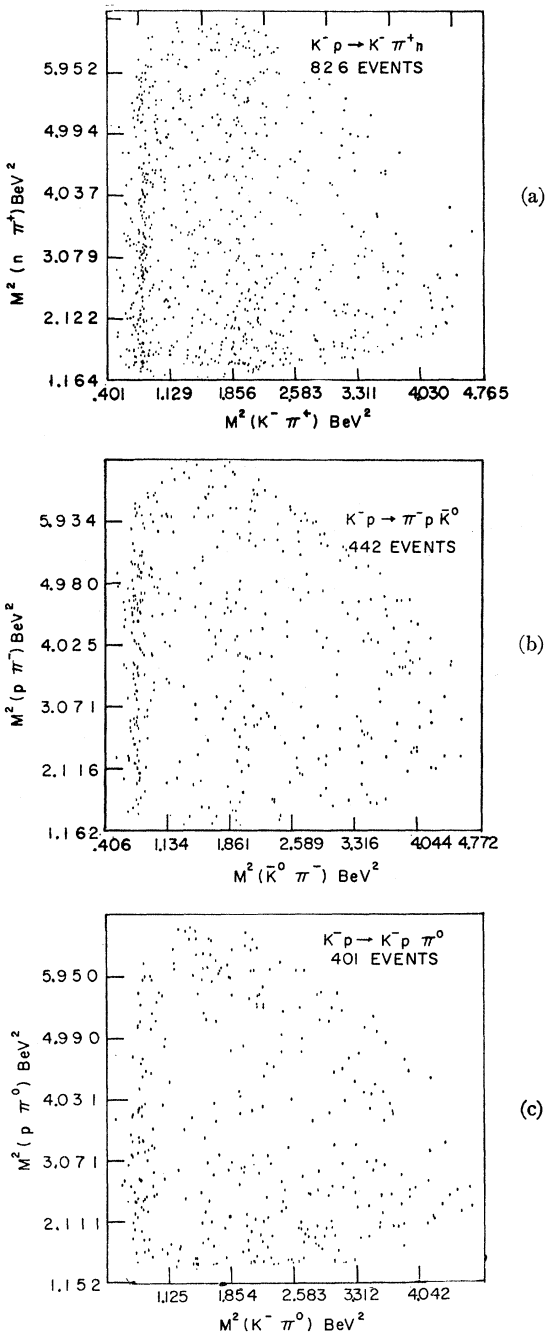

FIG. 5. Dalitz plots for the $N\pi$ invariant mass versus the $K\pi$ mass: (a) the final state $K^-\pi^+n$, (b) the final state $\pi^-p\bar{K}^0$, and (c) the final state $K^-p\pi^0$.

[12] For the final states (2) and (3) another background term (see Fig. 2) was included.

[13] A. H. Rosenfeld, N. Barash-Schmidt, A. Barbaro-Galtieri, L. R. Price, P. Söding, C. G. Wohl, M. Roos, and W. J. Willis, Rev. Mod. Phys. **40**, 77 (1968).

[14] The references for K^{*0}'s are Refs. 1 and 2 and the references for $K^{*-}(890)$ are as follows: G. W. London, R. R. Rau, N. P. Samios, S. S. Yamamoto, M. Goldberg, S. Lichtman, M. Primer, and J. Leitner, Phys. Rev. **143**, 1034 (1966), at 2.24 BeV/c; J. H. Friedman and R. R. Ross, Phys. Rev. Letters **16**, 485 (1966), at 2.45 and 2.64 BeV/c; Birmingham-Glasgow-London (I.C.)-München-Oxford-Rutherford Laboratory Collaboration RPP/H/25 (unpublished), at 6.0 BeV/c; and Ref. 1, at 4.1 and 5.5 BeV/c.

[15] D. R. O. Morrison, Phys. Letters **22**, 528 (1966).

section at 4.1 BeV/c has been suppressed by threshold effects.[16]

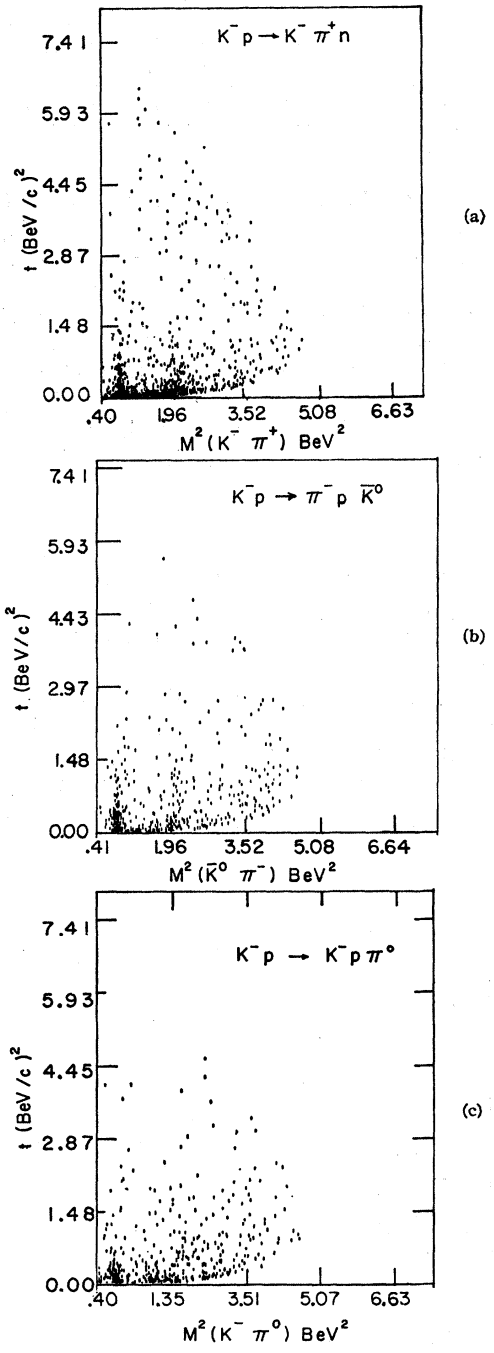

FIG. 6. Chew-Low plots: (a) the final state $K^-\pi^+n$, (b) the final state $\pi^-p\bar{K}^0$, and (c) the final state $K^-p\pi^0$.

[16] W. DeBaere, J. Debaisieux, P. Dufour, F. Grard, J. Neughebaert, L. Pape, P. Peeters, F. Verbeure, R. Windmolders. Y. Goldschmit-Clermont, V. P. Henri, B. Jongejans, A. Moisseev, F. Muller, J. M. Perreau, A. Prokes, and V. Yarba, Nuovo Cimento **51**, 401 (1967). The $K^*(1420)$ was observed in constructive interference with $N^*(1236)$.

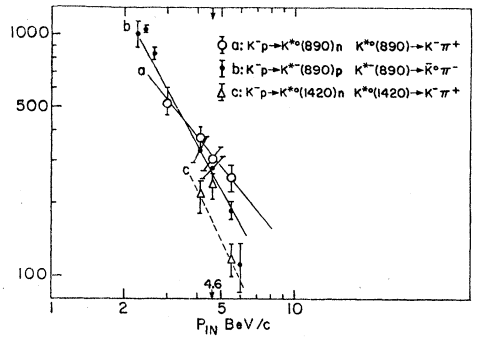

FIG. 7. The cross sections (μb) of K^* production as a function of incident momentum.

IV. $K^*(890)$

The $K^*(890)$ is produced relatively cleanly because the nonresonant background is less than 20% in the mass region 840 to 940 MeV. The four-momentum transfer was restricted to $|t|<0.5$ (BeV/c)^2 to purify the sample further.

The decay angular distributions of the K^*'s involve the spin density matrix elements, which are determined by the production process. Therefore, both the spin of the decaying particles and the production mechanisms can be studied by investigation of the decay angular distributions. In the K^* rest frame (the coordinate system is defined by choosing the z axis in the direction of the K^- incident beam particle and the y axis normal to the resonance production plane), the decay angular distribution of the $K^*(890)$ is

$$W_1(\theta,\varphi)=(3/4\pi)[\rho_{00}\cos^2\theta+\tfrac{1}{2}(1-\rho_{00})\sin^2\theta - \rho_{1,-1}\cos 2\varphi\sin^2\theta-\mathrm{Re}\rho_{10}\sqrt{2}\cos\varphi\sin 2\theta], \quad (4)$$

where θ is the polar angle of one of the decay particles and ϕ is the corresponding azimuthal angle [see Fig.

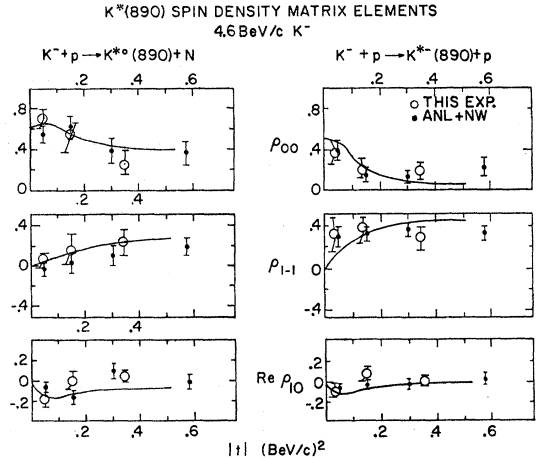

FIG. 8. Spin density matrix elements as a function of four-momentum transfer for $K^{*0}(890)$, produced in the reactions $K^-p\to K^{*0}(890)n$ and $K^-p\to K^{*-}(890)p$ at 4.57 BeV/c. The compared data are from Ref. 1. The curves are also from Ref. 1 and were calculated from the absorptive peripheral model.

TABLE I. Production cross sections, masses, and widths for K^*'s.

Reaction $K^-p\rightarrow$	Final-state cross section (mb)	$K^*(890)\rightarrow K^-\pi^+$ $\rightarrow \bar{K}^0\pi^-$ Mass (MeV)	Width (MeV)	Cross section (μb)	$K^{*0}(1420)\rightarrow K^-\pi^+$ Mass (MeV)	Width (MeV)	Cross section (μb)
$K^-\pi^+n$	1.222±0.112	899±5	48±8	306±34	1425±15	116±17	236±28
$\pi^-p\bar{K}^0$	0.704±0.124	884±5	52±8	279±29	...	...	...

9(c)]. The spin density matrix elements ρ_{00}, $\rho_{1,-1}$, and $\mathrm{Re}\rho_{10}$ are the three independent quantities which determine the form of the distribution. Conversely, their values may be inferred from the experimental distribution.

The spin density matrix elements can be expressed in terms of expectation values (or moments) of certain functions of θ and ϕ. These expressions were used to calculate the spin density matrix elements from the experimental distributions. The results are given in Table II. The ρ_{ij} are shown as a function of four-momentum transfer in Fig. 8 (Argonne-Northwestern results[1] at 4.1 BeV/c are also included). Both data are in good agreement with the theoretical curves from Ref. 1.

By integrating $W(\theta,\phi)$ over θ and ϕ separately, the distributions in θ and ϕ given are by

$$W(\theta)=\tfrac{3}{2}[\rho_{00}\cos^2\theta+\tfrac{1}{2}(1-\rho_{00})\sin^2\theta],$$
$$W(\rho)=(1/4\pi)(1-2\rho_{1,-1}\cos 2\phi). \quad (5)$$

In Figs. 9(a), 9(b), 10(a), and 10(b) are shown the experimental data and the distributions in θ and ϕ from Eq. (5) and Table II. It can be seen from Table II that for the $K^{*0}(890)$ for $|t|<0.2$ (BeV/c)^2, $W(\theta)$ is dominated by the $\cos^2\theta$ terms and $W(\theta)$ is nearly isotropic, while for $K^{*-}(890)$, $W(\theta)$ is dominated by the $\sin^2\theta$ term and $W(\phi)$ is a function of $\cos(2\phi)$. This suggests that the $K^{*0}(890)$ production is dominated by pseudoscalar exchange ($\rho_{00}\cong 1$), while the $K^{*-}(890)$ is produced by vector exchange ($\rho_{00}\cong 0$, $\rho_{1,-1}\neq 0$).

This conclusion is further supported by the production angular distributions shown in Figs. 9(d) and 10(c). The $K^{*0}(890)$ is seen to have a sharper forward peaking than the $K^{*-}(890)$, suggesting that a lighter particle is exchanged in the production process.

TABLE II. $K^*(890)$ spin density matrix elements.

Reaction	$K^-p\rightarrow K^{*0}(890)n$, $K^{*0}(890)\rightarrow K^-\pi^+$		
4-momentum transfer squared (BeV/c)^2	Spin density matrix elements ρ_{00}	$\rho_{1,-1}$	$\mathrm{Re}\rho_{10}$
$t<0.5$	0.519±0.072	0.143±0.066	−0.067±0.041
$t<0.1$	0.695±0.098	0.070±0.086	−0.178±0.075
$0.1\leq t<0.2$	0.516±0.166	0.170±0.156	0.013±0.094
$0.2\leq t<0.5$	0.277±0.123	0.229±0.129	0.041±0.056
	$K^-p\rightarrow K^*(890)p$, $K^{*-}(890)\rightarrow \bar{K}^0\pi^-, K^-\pi^0$		
$t<0.5$	0.206±0.061	0.282±0.072	0.067±0.030
$t<0.1$	0.350±0.130	0.295±0.151	−0.077±0.064
$0.1\leq t<0.2$	0.174±0.102	0.325±0.130	0.078±0.055
$0.2\leq t<0.5$	0.140±0.089	0.240±0.130	0.002±0.048

Since the total cross section for $K^-p\rightarrow K^{*0}(890)n$ is 459 μb, the total cross section for $K^-p\rightarrow K^{*-}(890)p$ due to the pion exchange alone is $\frac{1}{4}\times 459=115$ μb from isospin prediction. The cross section for $K^-p\rightarrow K^{*-}(890)p$ due to vector exchange alone is $393-115=278$ μb. Thus the pion exchange fraction is 29%. This value is consistent with $\rho_{00}=0.35$ in the region $|t|<0.1$ (BeV/c)^2 where the pion exchange production is dominant (see Table II). Hence, the vector-meson exchange dominance in the $K^{*-}(890)$ production is indicated by isospin arguments.

V. $K^{*0}(1420)$

The $K^{*0}(1420)$ is dominantly produced at low four-momentum transfer: $|t|<0.2$ (BeV/c)^2. Nonresonant background is about 40% in the mass region 1330 to 1510 MeV.

The $K^{*0}(1420)$ decay angular distributions for two four-momentum transfer regions are shown in Figs. 11(a) and 11(b). We notice, first, that after the background substraction (using the neighboring bins: 1240 to 1330 and 1510 to 1600 MeV), the sharp forward peak-

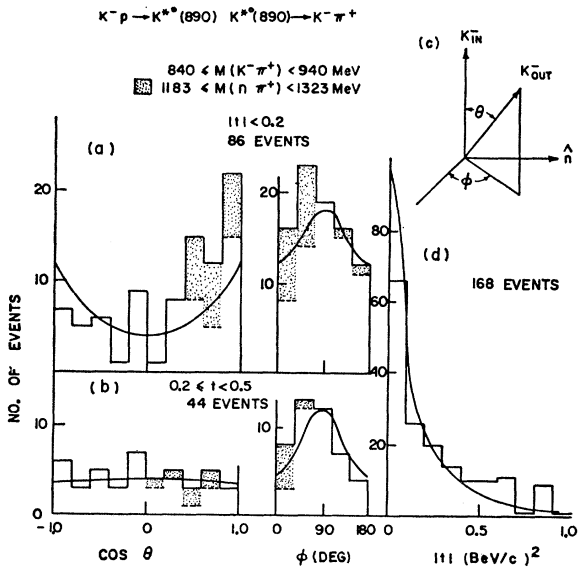

FIG. 9. The decay angular distributions for (a) $|t|<0.2$ (BeV/c)^2 and (b) $0.2\leq|t|<0.5$ (BeV/c)^2, and (d) four-momentum transfer distribution for $K^{*0}(890)$ produced in the reaction $K^-p\rightarrow K^{*0}(890)n$. The selected resonance mass region is $840\leq M(K^-\pi^+)\leq 940$ MeV/c^2. The absorption model curve (d) is from Ref. 1.

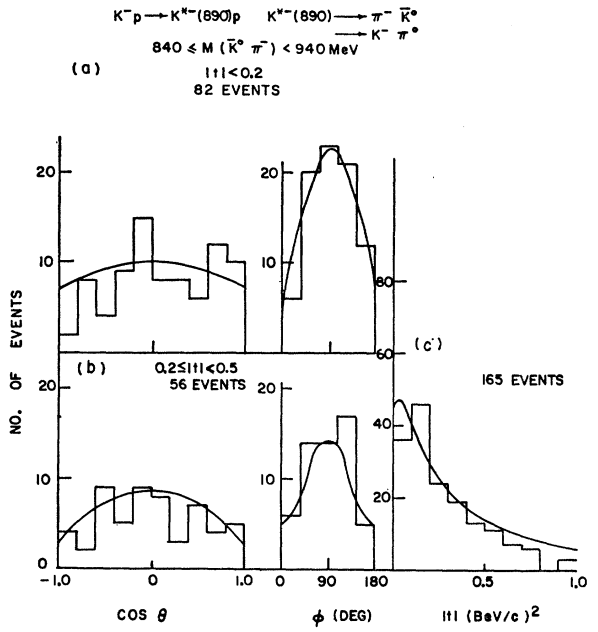

FIG. 10. The decay angular distributions for (a) $|t|<0.2$ $(\mathrm{BeV}/c)^2$, (b) $0.2\leq|t|<0.5$ $(\mathrm{BeV}/c)^2$, and (c) four-momentum transfer distribution for $K^{*-}(890)$ produced in the reaction $K^-p \to K^{*-}(890)p$. The selected resonance mass region is $840\leq M(K\pi)\leq 940$ MeV/c^2. The absorption model curve in (c) is from Ref. 1.

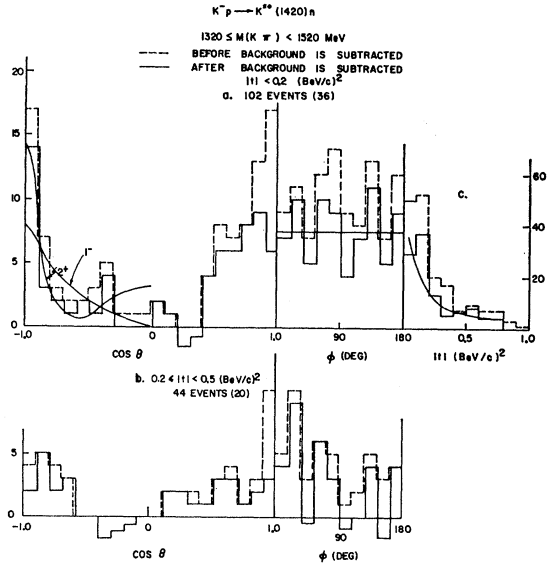

FIG. 11. The decay angular distributions for (a) $|t|<0.2$ $(\mathrm{BeV}/c)^2$ and (b) $0.2\leq|t|<0.5$ $(\mathrm{BeV}/c)^2$, and (c) four-momentum transfer distribution for $K^{*0}(1420)$ produced in the reaction $K^-p \to K^{*0}(1420)n$. The selected resonance mass region is $1330 \leq M(K^-\pi^+)\leq 1510$. The background mass regions are $1240 \leq M(K^-\pi^+)<1330$ MeV/c^2 and $1510\leq M(K^-\pi^+)<1600$ MeV/c^2. The absorption model curve in (c) is from Ref. 14, and normalized to the experimental data. The numbers in parentheses following event numbers indicate background events.

ing in the $\cos\theta$ distribution disappears, while the sharp backward peaking remains. This is contrasted to the $K^{*0}(890)$ case where the forward-backward symmetry was somewhat recovered after the $N^*(1236)$ subtraction. This asymmetry may be related to interference with N^*'s. We notice secondly that the distribution in $\cos\theta$ for $|t|<0.2$ $(\mathrm{BeV}/c)^2$ is quite different from that for $0.2\leq|t|<0.5$ $(\mathrm{BeV}/c)^2$. The sharp backward peaking, plus a comparison of the number of K^* events and background fractions in the two momentum regions [see Figs. 11(a) and 11(b)], suggests that $K^{*0}(1420)$ is dominantly produced in the region $|t|<0.2$ $(\mathrm{BeV}/c)^2$.

The preferred spin-parity assignment for the $K^*(1420)$ as reported in previous experiments is 2^+, but the 1^- possibility has not been ruled out.[17] For spin-parity 1^- the decay angular distribution is given by Eq. (4), while the distribution for 2^+ is given by

$$\begin{aligned} W_2(\theta,\phi) = (15/16\pi)\{&[\rho_{22}\sin^4\theta+\rho_{11}4\sin^2\theta\cos^2\theta \\ &+\rho_{00}\tfrac{1}{3}(3\cos^2\theta-1)^2]+\cos2\phi\,[\rho_{20}(\tfrac{2}{3}\sqrt{6}) \\ &\times\sin^2\theta\,(3\cos^2\theta-1)-\rho_{1,-1}4\sin^2\theta\cos^2\theta] \\ &+\cos\phi\,[-\rho_{21}4\sin^3\theta\cos\theta-\rho_{10}(\tfrac{4}{3}\sqrt{6}) \\ &\times(3\cos^2\theta-1)]+\cos3\phi\,[\rho_{2,-1}4\sin^3\theta\cos\theta] \\ &+\cos4\phi\,[\rho_{2,-2}\sin^4\theta]\}. \quad (6) \end{aligned}$$

The eight spin density matrix elements were experimentally determined by the moment method described in the $K^*(890)$ case, and the results are shown in Table III.

[17] The earlier references are found in Ref. 1.

The curves for 1^- and 2^+ in Fig. 11(a) were drawn by using only the dominant ρ_{00} contributions in Table III. The 2^+ curve fits the present data better than the 1^- curve. Events in the backward region (in our coordinate system) can be interpreted as pure K^* events because N^* events and diffraction scattering events do not contribute in this region, and general background events are distributed isotropically in $\cos\theta$. It should be noted that the value $\rho_{00}\simeq 1$ for 1^- is the physical upper limit for ρ_{00}, and the last bin is more than two standard deviations above this upper limit for the 1^- curve. Thus, the sharp backward peaking which is characteristic of a $\cos^4\theta$ component suggests 2^+.

It is seen in Table III that all matrix elements except ρ_{00} and ρ_{11} are very small. Pion exchange with absorption predicts $\rho_{00}=0.87$, $\rho_{11}=0.06$, and all other $\rho_{ij}=0$, while vector exchange with absorption predicts $\rho_{11}=0.4$ and all others small.[18] Our data, therefore, suggest that the production mechanism of the $K^{*0}(1420)$

TABLE III. $K^{*0}(1420)$ spin density matrix elements.

Spin-parity	Spin density matrix elements ρ_{00}	$\rho_{1,-1}$	ρ_{10}	ρ_{11}
1^-	0.996 ± 0.073	0.052 ± 0.071	0.011 ± 0.047	...
2^+	0.761 ± 0.093	0.038 ± 0.083	-0.002 ± 0.010	0.352 ± 0.036
	ρ_{21}	ρ_{20}	$\rho_{2,-1}$	$\rho_{2,-2}$
2^+	0.007 ± 0.032	-0.004 ± 0.045	0.040 ± 0.043	0.021 ± 0.062

[18] H. Högaasen, J. Högaasen, R. Keyser, and B. E. Y. Svensson, Nuovo Cimento 42, 323 (1966).

in the present experiment is dominantly pion exchange with some admixture of vector-meson exchange since ρ_{11} is much larger than the predicted value of 0.06. The distribution in ϕ is approximately isotropic and is consistent with this conclusion. The value ρ_{22}, calculated by the normalization condition $\rho_{00}+2\rho_{11}+2\rho_{22}=1$, is -0.233 ± 0.083. A large negative value of ρ_{22} was obtained by workers for the f^0 meson.[19] The unphysical negative value of ρ_{22} is interpreted in the present experiment as due to the large background for which only an approximate correction can be made.

The production angular distribution in Fig. 11(c) indicates a broader forward peaking than for $K^{*0}(890)$. This is partly due to a higher kinematic limit in the 1400-MeV region (see Chew-Low plot). The theoretical curve shown fits the shape of the data but was normalized to the total number of events.[16]

VI. CONCLUSIONS

The $K^*(890)$ production is prominent in all three reactions, while the $K^*(1420)$ is produced most copiously in the final state $K^-\pi^+N$. The $K^*(890)$ is produced with a signal-to-background ratio of better than 4 to 1. The decay and production angular distributions suggest that the $K^{*0}(890)$ is dominantly produced by pion exchange, while the $K^{*-}(890)$ production mechanism is dominantly ω exchange. This conclusion is consistent with the isospin prediction that for pure $T=1$ pseudoscalar exchange the cross section for $K^{*0}(890)$ production is four times as large as that for the $K^{*-}(890)$ production. The $K^{*0}(1420)$ is dominantly produced at low momentum transfers, $|t|<0.2$ BeV/c. The cross section for $K^{*0}(1420)$ production at 4.57 BeV/c appears to be higher than the value which the data at other momenta suggest. This may possibly be explained by threshold effects. The study of the spin density matrix elements also indicates that pion exchange is dominant in $K^{*0}(1420)$ production. We favor a spin-parity assignment of 2^+ for the $K^*(1420)$ on the basis of our analysis.

ACKNOWLEDGMENTS

The author is grateful to Professor W. J. Kernan for suggesting this problem and for his continued encouragement. He also wishes to thank Dr. J. I. Rhode and Dr. R. A. Leacock for many useful discussions. A great effort by the scanning, measuring, and programming staffs is acknowledged.

[19] J. A. Poirier, N. N. Biswas, N. M. Cason, I. Derado, V. P. Kenney, W. D. Shephard, E. H. Synn, H. Yuta, W. Selove, R. Ehrlich, and A. L. Baker, Phys. Rev. **163**, 1462 (1967); H. O. Cohn, R. D. McCulloch, W. H. Bugg, and G. T. Condo, Nucl. Phys. **82**, 690 (1966).